Single-Transistor Impedance Matching Circuit for Over-Hundred-Octave Active Antennas

Shuyu Wang and Yue Li, *Senior Member, IEEE*

***Abstract*— In this article, a novel active impedance matching circuit with a single transistor is studied for antennas to cover over a hundred-octave bandwidth. In the proposed matching circuit, only one field effect transistor (FET) is utilized and biased in the ohmic region. The FET is integrated with a dipole antenna at the gate, and connected with a 50 Ω transmission line at the drain. With small dimensions, this active antenna performs as a receiver with a wide impedance bandwidth of 10 MHz–1.9 GHz, in which the reflection coefficient is lower than −10 dB, covering 190 octave bandwidth. An equivalent circuit model of the ohmic-biased FET is built to analyze this unusual wideband performance, which exhibits promising applications in ultrawideband (UWB) electromagnetic sensing systems with extremely restricted volume.**

***Index Terms*— Active wideband antennas, field effect transistors (FETs), hundred octave, impedance matching circuit, ohmic region.**

I. Introduction

BANDWIDTH of impedance, i.e., the operating frequency range of impedance matching with low reflection loss, is one of the most critical criteria in evaluating the performance of an antenna [1], [2], [3], [4], [5]. Wideband antennas possess significant benefits, such as multiple mode sensing, high multipath resolution, high spectrum efficiency, and noise immunity, to name a few [6], [7], [8], [9]. Therefore, expanding the bandwidth of antennas has been a constant pursuit in antenna engineering [5], [10]. Over the last decades, numerous studies have validated a limit on the antenna's achievable bandwidth over certain dimensions, which is known as Chu's limit [11], [12], [13]. On the other hand, impedance matching is a critical method to enhance an antenna's bandwidth without enlarging its dimensions. But there is still a bandwidth limit for certain antenna impedance cooperated with a passive matching circuit, known as the Bode-Fano limit [14], [15]. As the Bode-Fano limit indicates, the antennas with electrically small dimensions possess a large capacitive impedance, while their achievable bandwidth is still narrower even with a passive matching network [16]. Under these restrictions, wideband antennas are not realized with electrically small dimensions, restricting their applications in volume-limited systems, especially for multiantenna scenarios [17], [18], [19], [20].

As a feasible approach to breaking the limit between bandwidth and dimension, the active antennas have caught the focus [21], [22], [23], [24]. The active antennas utilize active impedance matching circuits with biased transistors to enhance the impedance bandwidth without increasing their dimensions. These active impedance matching circuits can be categorized into two classifications, non-Foster circuits and amplifier integration. The non-Foster circuits, as the negative-impedance matching circuits, provide negative capacitance or inductance to cancel the reactance of a passive antenna in a relatively wide bandwidth. Numerous studies on the non-Foster circuits have been carried out in [25], [26], [27], [28], and [29]. For example, in [28], an active dipole antenna with a length of $0.07\lambda_0$ (λ_0 is the vacuum wavelength of the electromagnetic wave at the center frequency) is realized with a bandwidth of 6 octaves (20–120 MHz). Amplifier integration is another widely adopted method for active antennas [30], [31], [32], [33], [34], [35]. By integrating the passive antennas with power amplifiers (PAs) or low-noise amplifiers (LNAs), antennas obtain improvement in bandwidth and gain. Foroutan and Nikolova [30] integrate a slot antenna with an LNA chip for ultrawideband (UWB) applications. In [32], a transmitting amplifier is utilized to match a dipole antenna with $0.03\lambda_0$ length, reaching a bandwidth of 7.3 octaves (3–22 MHz). In summary, both methods of non-Foster circuits and amplifier integration are able to provide wideband impedance matching for electrically small antennas. However, these existing active matching circuits are unable to work if wider bandwidth is further required, e.g., over 10 octaves. Therefore, further expanding the active antennas' bandwidth beyond the existing methods is still pursued with significant requirements.

In this article, a novel active impedance matching circuit is proposed for realizing the over-hundred-octave antennas. The proposed active matching circuit consists of a single field effect transistor (FET) as the core element. In the utilization, an antenna is connected to the gate of the FET, and the feeding transmission line connects to the drain. Biasing voltage and elements are designed to ensure an ohmic-region operation of FET. For performance demonstration, a dipole antenna with a small dimension is used as an example. Utilizing the proposed active ohmic-FET matching circuit, an ultrawide bandwidth of 10 MHz–1.9 GHz is realized, covering a 190 octave bandwidth. A prototype of the antenna with the ohmic-FET

Manuscript received 4 November 2023; revised 16 December 2023; accepted 3 January 2024. Date of publication 15 January 2024; date of current version 7 March 2024. This work was supported in part by the National Natural Science Foundation of China under Grant U22B2016 and in part by the National Key Research and Development Program of China under Grant 2021YFA0716601. *(Corresponding author: Yue Li.)*

The authors are with the Department of Electronic Engineering and the Beijing National Research Center for Information Science and Technology, Tsinghua University, Beijing 100084, China (e-mail: lyee@tsinghua.edu.cn).

Color versions of one or more figures in this article are available at https://doi.org/10.1109/TAP.2024.3351203.

Digital Object Identifier 10.1109/TAP.2024.3351203

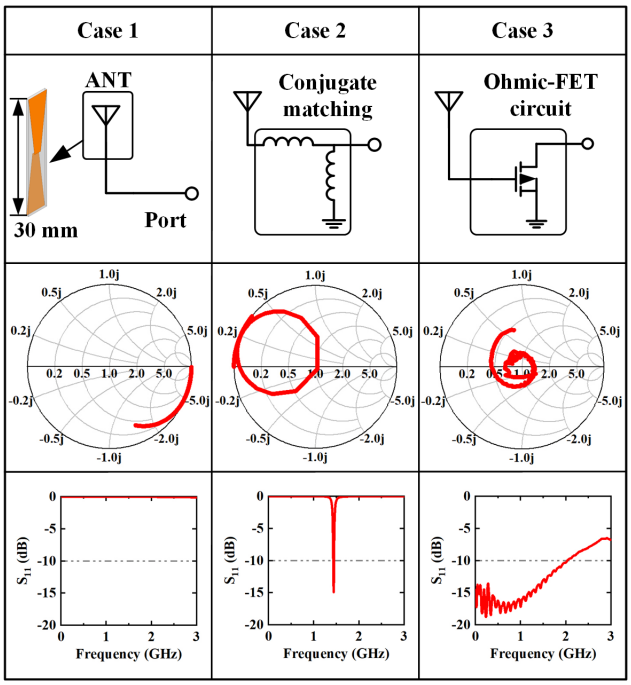

Fig. 1. Comparison of general schematics, Smith charts, and reflection coefficients of antennas without matching, using conjugate matching, and the proposed ohmic-FET matching circuit.

matching circuit is fabricated and tested, verifying the UWB performance of the active matching circuit.

II. Impedance Matching With Ohmic-FET

A. Ohmic-FET Matching Mechanism

Impedance matching is a critical procedure in expanding the bandwidth of antennas, while the most widely applied matching mechanism is conjugate matching. However, restricted by the Bode-Fano limit, impedance matching with a passive circuit is only realized in a narrow bandwidth for an electrically small antenna. Fig. 1 shows the performances of different cases, in which the antenna is without or with the impedance matching circuit. Two different impedance matching circuits include the passive conjugate matching circuit and the proposed active ohmic-FET circuit. As an example, a dipole antenna with a length of 30 mm is examined in the 10 MHz–3 GHz frequency range ($\lambda_0 = 30$ m–100 mm). In case 1, the antenna is directly connected to the feeding port without any matching circuits. As shown in the Smith chart, the dipole antenna with a smaller dimension compared to the operation wavelength performs with a nearly pure capacitive impedance. Thus, the impedance is not surprisingly mismatched with the resistive 50 Ω port. The reflection coefficient is shown, where the S11 is nearly 0 dB throughout the band. In this case, almost all of the fed power is reflected back to the source. Case 2 shows the performance of the same antenna with a passive conjugate matching circuit. As illustrated in the schematic in Fig. 1, a pair of serial and shunt inductors are used to match the antenna. The Smith chart indicates a matched impedance in a narrow bandwidth. The reflection coefficient of the antenna shows an impedance matching in a narrow bandwidth of 1.4%. The results validate that conjugate matching operates only in a narrow bandwidth. To enhance the bandwidth over the conjugate matching, an active circuit based on a single ohmic-FET is proposed for wideband impedance matching. As illustrated in case 3, the same dipole antenna is directly connected to the gate of FET. The FET's drain is connected to the feeding port. As the unique feature of this approach, the FET is biased in the ohmic region, such that a 50 Ω impedance at the drain is configured in a relatively wide bandwidth. The reflection coefficient indicates an operation bandwidth of 10 MHz–2.03 GHz (198%), which is much wider than the achievable bandwidth with conjugate matching, indicating the unique ability of wideband impedance matching beyond the classical limits for antennas.

B. Circuit Model of FET Biased in Ohmic Region

The proposed active ohmic-FET matching circuit is different from the conventional circuit designs with FETs as amplifiers. Three major differences are discussed here to distinguish the ohmic-FET circuit from the conventional amplifier-integrated circuits. First, the ohmic-FET circuit operates as an active matching network itself and therefore requires no extra impedance matching elements or circuits at the gate or at the drain. However, the amplifiers aim for signal amplification and therefore demand extra input and output matching circuits. The second difference lies in the operation regions of FET. The FET in our proposed active matching circuit is biased in the ohmic region to ensure a stable resistive impedance across a wide range of spectrum, while in the amplifier, the FETs operate in the saturation region to ensure a high gain. Third, the amplifiers require a feedback loop to ensure circuit stability. However, the ohmic region of the FET is intrinsically stable and requires no extra feedback.

To reveal the operation mechanism of the active ohmic-FET impedance matching circuit, an equivalent circuit model of the ohmic-biased FET integrated with an antenna is illustrated in Fig. 2(a). As depicted in case 1 of Fig. 1, the passive antenna with an electrically small dimension possesses a large capacitive impedance. Therefore, the antenna can be modeled as a voltage source V_A with an internal capacitor C_A, under the scenario of electromagnetic wave receiving. The voltage V_A represents the electrical potential that the antenna coupled from the free space. According to the working mechanism, the drain current of FET is controlled by this voltage at the gate. Therefore, the FET is equivalent to a voltage-controlled current source g_m with its related parasitic elements. The insulator of the gate is modeled with the gate capacitor C_G. The channel of the FET possesses a frequency irrelevant conductivity, thus is modeled with a drain resistor R_D, while a drain capacitor C_G is introduced by the semiconductor between the drain and the source.

C. Matching Circuit Design Procedure

As illustrated in Fig. 2(b), the equivalent model of the ohmic FET matching circuit can be divided into three parts, including the input part, the transmission part, and the output part. The input part consists of the source V_A, the antenna capacitance C_A, and the gate capacitance C_G. The antenna capacitance and

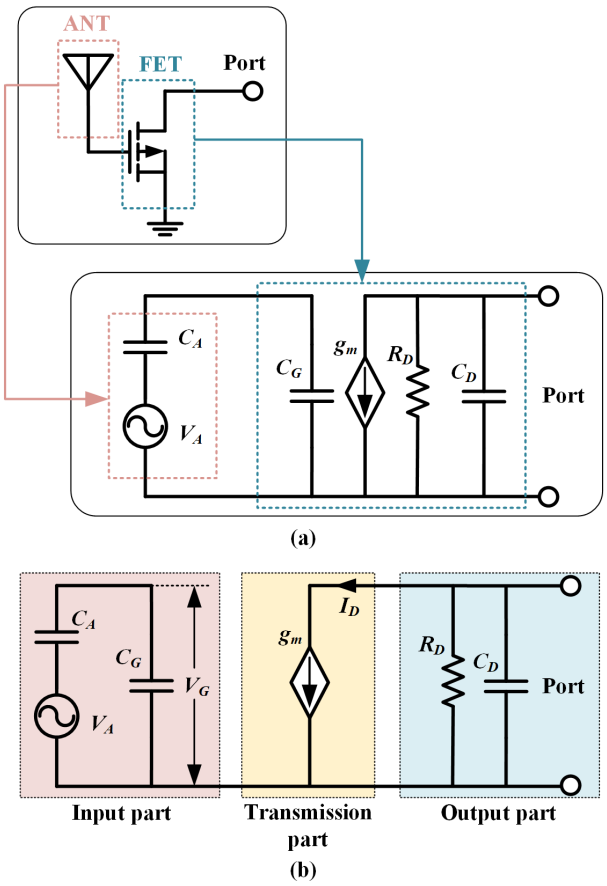

Fig. 2. (a) Equivalent circuits of the ohmic-FET matching circuit. (b) Input, transmission, and output parts of the equivalent circuit model.

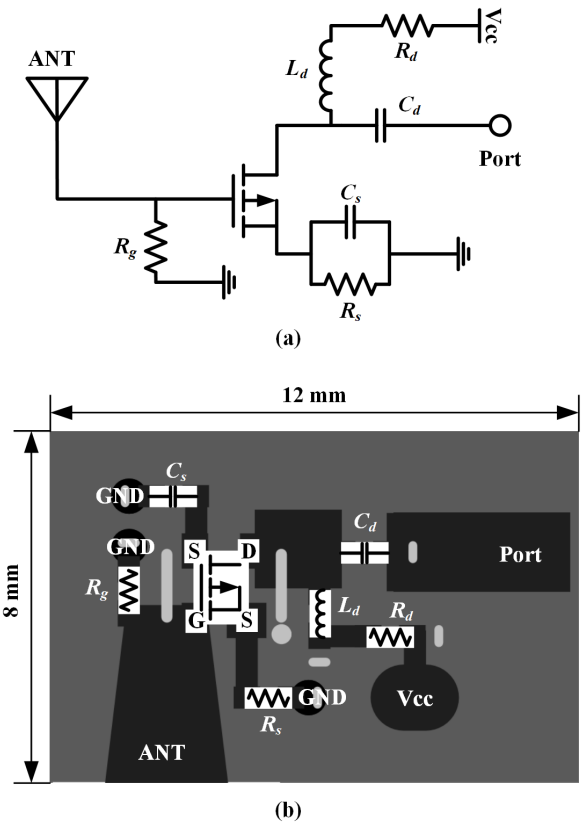

Fig. 3. Design of the ohmic-FET matching circuit. (a) Schematic and (b) circuit board diagram.

the gate capacitor form a serial voltage division. Therefore, the gate voltage yields $V_G = V_A \times C_A/(C_A + C_G)$. This part describes that the gate voltage is controlled by the antenna's voltage through field coupling rather than the current coupling. The transmission part consists of the voltage-controlled current source g_m. Through this part, the bias voltage is transformed into the modulated drain current of $I_D = g_m \times V_G$. The transmission part outlines that the drain current is linearly controlled by the gate voltage with field effect. The output part consists of the drain resistor R_D and drain capacitor C_D. The drain impedance is expressed as $Z_D = R_D - j/(\omega C_D)$. The drain resistor represents the channel resistance that is configured by the biasing voltage. On the other hand, the drain capacitance is determined by the substrate between the drain and the source. In the lower frequency band, an arbitrary resistance can be achieved by configuring the FET in the ohmic region, including the frequently used 50 or 75 Ω of transmission lines. However, with the increase in frequency, the drain capacitance has a significant impact on impedance, which causes a mismatch at the higher frequency and limits the operation bandwidth of the matching circuit.

The schematic of the ohmic-FET with bias elements is illustrated in Fig. 3(a). The gate works as the input port which connects with the passive antenna, with the drain working as the output port. Resistors R_g, R_s, and R_d, are connected to the gate, source, and drain respectively for the configuration of biasing voltages. Blocking capacitors C_s and C_d, and choking inductor L_d decouples the interference between the RF signal and the dc bias. The procedure for evaluation of the element values is summarized as follows. First, a bias point is determined from the I–V curve of the utilized FET. This bias point is chosen at $V_{GS} = -0.14$ V, $I_D = 0.14$ mA, and $V_{DS} = 0.7$ V, where the output impedance is 50 Ω. Second, the values of the biasing resistors are calculated. R_G is set at 10 kΩ to ensure a 0 V dc gate voltage. R_S is $-V_{GS}/I_D = 10$ Ω and R_D is set at 110 Ω. Therefore, biasing voltage Vcc $= -V_{GS} + V_{DS} + I_D \times R_D = 2.4$ V. Finally, the choking inductor L_d of 180 nH and blocking capacitors C_s and C_d of 4.7 nF are chosen to minimize the influence on the FET's impedance. The values of each element are listed in Table I. The circuit board diagram is shown in Fig. 3(b), where the gate, source and drain of the FET are denoted G, S, and D. The entire matching circuit is printed on a printed circuit board (PCB) with a dimension of 12 × 8 mm.

TABLE I
ELEMENT VALUES OF THE OHMIC-FET CIRCUIT

R_g	R_s	R_d	C_s	C_d	L_d
10 kΩ	10 Ω	110 Ω	4.7 nF	4.7 nF	180 nH

III. ANTENNA DESIGN AND SIMULATION RESULTS

A. Antennas With Ohmic-FET Matching Circuit

As a demonstration of impedance matching capabilities, a printed dipole antenna is integrated with the ohmic-FET circuit as an example. To testify to the performances of this

active matched antenna, numerical simulations are conducted. The simulation process consists of two parts, namely the full-wave simulation and the circuit simulation. Full-wave simulation is conducted on the passive dipole antenna without a matching circuit. The simulations are run with the software Ansoft HFSS 18.0, and the impedance result is exported for circuit simulations. The circuit simulations are run with Cadence AWR. Because the ohmic region has been seldom adopted in previous works, datasets of ohmic-FETs are not provided. Therefore, an ohmic-FET circuit is fabricated and measured. The S-matrix of the ohmic-FET is extracted and connected to the passive antenna impedance in the circuit simulations. The impedance bandwidth of the matched antenna is thereby acquired. The conceptual graph of the ohmic-FET is illustrated in Fig. 4(a) with parts labeled. By choosing different FET elements, the gate width W_g can be altered. A dipole antenna with the ohmic-FET matching circuit is printed on an FR-4 epoxy board ($\varepsilon_r = 4.4$, $\tan\delta = 0.02$) with 0.6 mm thickness. The dipole antenna has a length l_1 and width l_4, and the ohmic-FET matching circuit has length l_3 and width l_2. One arm of the dipole antenna directly connects to the solder pad of the FET's gate. The printed circuit is identical to Fig. 3(b) with soldered elements. Black, yellow, and green bocks denote resistors, capacitors, and inductors, respectively. The other arm of the dipole is printed together with the ground plane of the ohmic-FET circuit. The top and bottom views of the matched antenna are illustrated in Fig. 4(b) and (c). This antenna with an ohmic-FET matching circuit has an overall dimension of $30 \times 12 \times 0.6$ mm, indicating a miniaturized volume occupation as electrically small antennas. It is worth mentioning that although fed by an unbalanced microstrip line, the antenna does not require balun for operation. The proposed dipole antenna operates on voltage coupling with the ohmic-FET, without the need for current balance considerations. Moreover, the antenna has an electrically small size, causing its current on the antenna to be weak and neglectable.

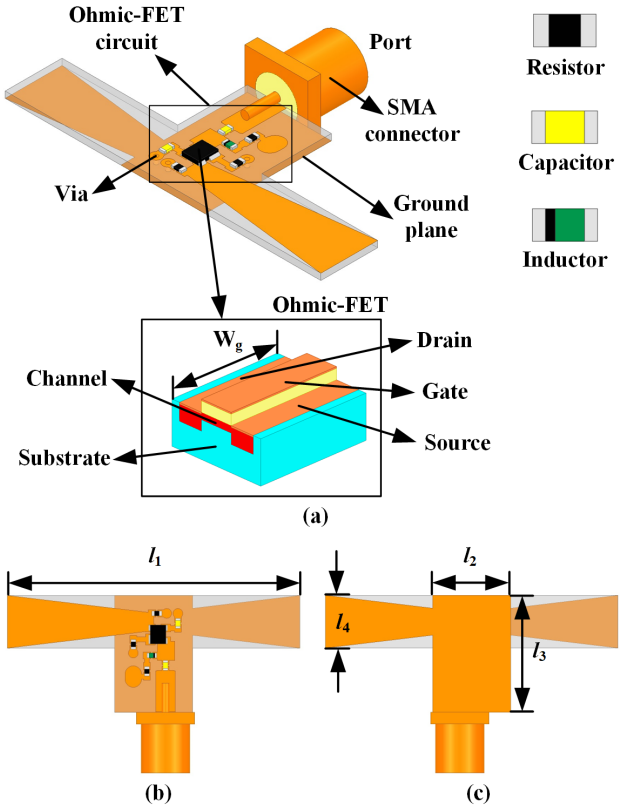

Fig. 4. General configuration of the proposed antenna with ohmic-FET matching circuit. (a) Perspective view, (b) top view, and (c) bottom view. Designed dimensions are $l_1 = 30$ mm, $l_2 = 8$ mm, $l_3 = 12$ mm, $l_4 = 5.4$ mm, and $W_g = 400$ μm.

B. Parameter Study on Antenna Performance

Based on the equivalent circuit model, the primary factors that determine the proposed ohmic-FET matching circuit and the antenna's performances are studied. As analyzed afore, the drain impedance of the FET is the sum of the channel resistance and drain capacitance. In the lower band, the effect of the drain capacitor is neglected, while as the frequency increases, the reactance of the drain capacitor increases significantly and causes an impedance mismatch with the resistive transmission line. Accordingly, it is analyzed that lowering the drain capacitor expands the matching bandwidth of this matched antenna at the higher band. The drain capacitor is introduced by the substrate between the drain and the source. Therefore, a feasible way to reduce the drain capacitor is to lower the width of the FET (denoted gate width, W_g), thereby reducing the effective surface area of the drain capacitor, and expanding the matching bandwidth of the matched antenna. To validate the analysis, the effect of the FET gate width on the impedance-matched bandwidth is studied. Here, three different high electron mobility transistors (HEMTs) NE3508M04 ($W_g = 800$ μm), NE3509M04 ($W_g = 400$ μm), and NE3510M04 ($W_g = 260$ μm) with different gate width and identical gate length are utilized as the ohmic-FETs to match the same antenna, respectively. The input gate impedances and the output drain impedances of the three utilized FETs are illustrated in Fig. 5. The real and imaginary part of the input port indicate a typical capacitive impedance. The output impedance is close to 50 Ω in an ultrawide bandwidth. From the measured impedances, the S-matrix of the ohmic-FETs are extracted and applied for simulation of matched antennas. The bandwidths of the antennas matched with different ohmic-FETs are depicted in Fig. 6. The maximum operation frequencies of the matched antennas are 1.54 GHz ($W_g = 800$ μm), 2.03 GHz ($W_g = 400$ μm), and 2.5 GHz ($W_g = 260$ μm), respectively, with reflection coefficients lower than -10 dB. It is observed that the impedance bandwidth expands to a higher band as the gate width of the ohmic-FET decreases. Therefore, it is reasonably assumed that decreasing the gate width of the FET would provide the ohmic-FET circuit with better high-frequency matching.

Furthermore, the overall gain of the antenna, i.e., the power output of the active circuit, is proportional to the gate voltage, which is a division of the electrical potential coupled by the antenna from the free space. According to the equivalent circuit model of the ohmic-FET matched antenna in Fig. 3, the gate voltage is inversely proportional to the dipole antenna's capacitance. For electrically small dipole antennas [36], its capacitance decreases as its length increases. Therefore, enlarging the dimensions of the dipole would raise the divided voltage of the gate, and therefore elevate the overall

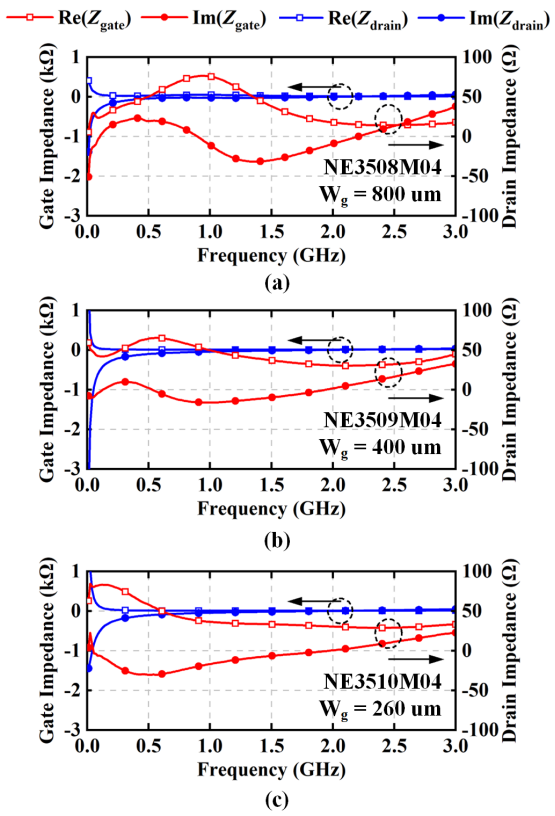

Fig. 5. Measured impedances of the input port (gate) and output port (drain) of the ohmic-FET matching circuit utilizing FETs with gate width (a) W_g = 800 μm, (b) W_g = 400 μm and (c) W_g = 260 μm.

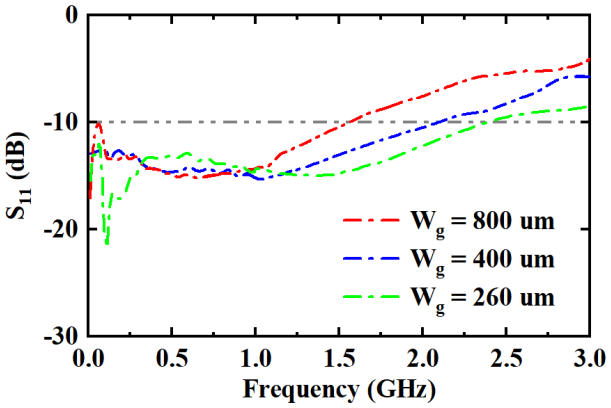

Fig. 6. Study on the influence of FET gate widths on the operation bandwidths.

gain. Gains of the matched antennas with lengths l of 20, 30, and 40 mm are illustrated in Fig. 7. It is showcased that the overall gain of the across the spectrum increases as the dipole antenna lengthens, reaching maximum gains of 2.5 dBi (20 mm), 3.0 dBi (30 mm), and 5.6 dBi (40 mm), respectively. The simulation results exceed the maximum gain a dipole antenna. As shown in the equivalent circuit model in Fig. 3(b), the channel converts the gate voltage to the drain current at the transmission part. It is known that comparing to LNAs with saturation FETs, the transmission coefficient of the ohmic-FET is low. However, the transmission coefficient is above 1 and extra gain is provided for the antenna beside the enhancement from impedance matching. Therefore, the

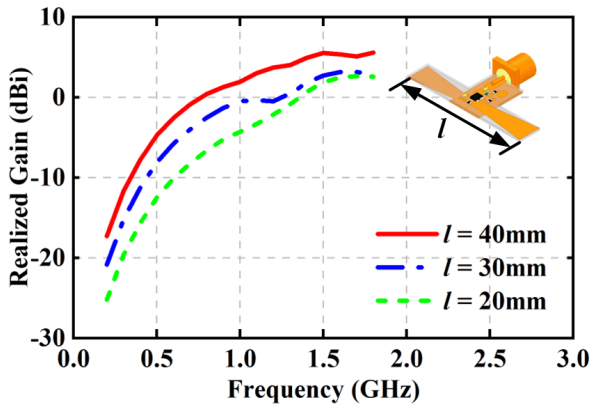

Fig. 7. Study on the influence of antenna length l on the gain.

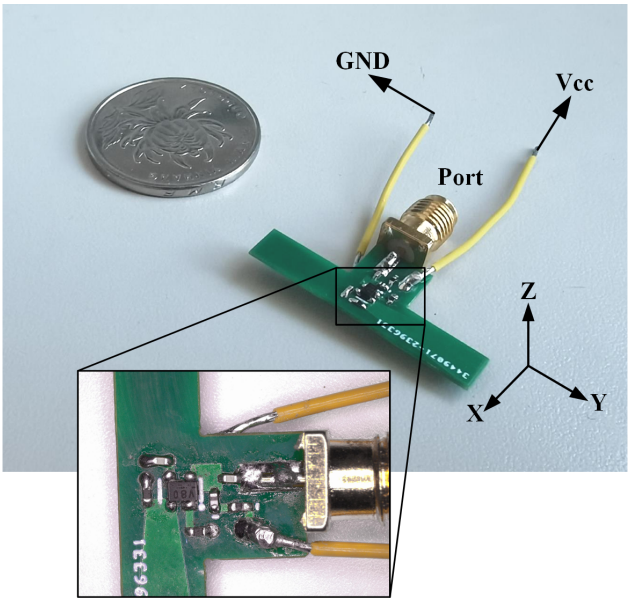

Fig. 8. Photograph of the fabricated antenna and the ohmic-FET matching circuit.

reachable gain of the matched dipole exceeds the dipole's limitations. Moreover, the results indicate that a feasible way to enhance the gain performance of the matched antenna is enlarging its dimensions, at the cost of volume occupation.

IV. Experiment Results

To verify the availability of the proposed matching circuit and the active antenna design, a prototype of the proposed antenna integrated with the ohmic-FET circuit is built and measured. The perspective view of the fabricated antenna is shown in Fig. 8, also with a zoomed-in view of the ohmic-FET matching circuit. The prototype consists of the ohmic-FET matching circuit and the dipole antenna. Copper is printed on both sides of an FR-4 epoxy board, with solder pads on the top and ground plane on the bottom. Electronic elements are soldered on the top of the antenna according to the circuit diagram in Fig. 4. A pair of feeding wires are soldered to the feeding pad and the ground, respectively, to provide the biasing voltage for the ohmic-FET. A coaxial SMA connecter is used as the feeding port. During experiments, the antenna is biased with a dc voltage source of 2.4 V and 14 mA output,

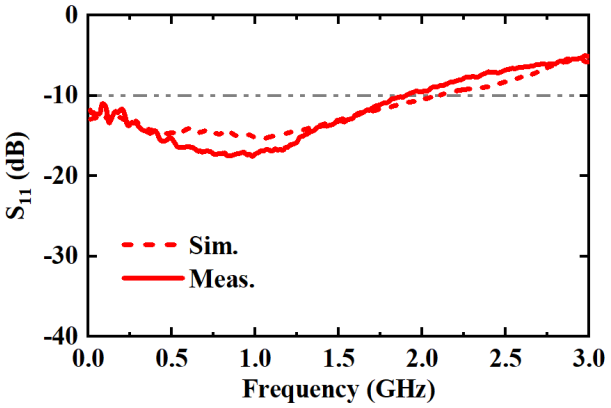

Fig. 9. Measured and simulated S-parameters of the proposed antenna.

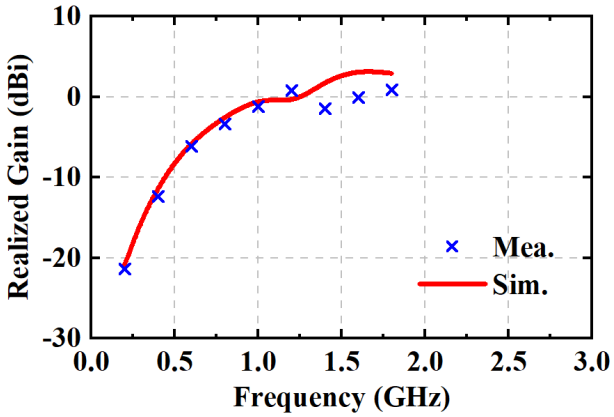

Fig. 10. Realized gain of the proposed antenna.

consuming an overall dc power of 33.6 mW. The reflection coefficient of the antenna was characterized by an Agilent N9917A vector network analyzer. The measured reflection coefficient is depicted in Fig. 9, compared with the simulation result. An impedance bandwidth of 10 MHz–1.9 GHz is realized with reflection coefficient lower than −10 dB, agreeing well with the simulation. The measured results validate the ability of the proposed ohmic-FET matching circuit to achieve superior bandwidth over existing methods.

The radiation patterns and gain were measured by comparing the received power of the proposed antenna to a half-wavelength dipole antenna. The half-wavelength dipole antennas are used as standard antennas, with their gains $G_{\text{dipole}}(f)$ measured in the anechoic chamber. The measurement procedure is as follows. First, a single-frequency wave is radiated using the signal generator and a half-wavelength dipole antenna. Another identical antenna is connected to the spectrum analyzer to receive this signal with received power P_1. Second, the receiving antenna is changed to the proposed antenna, with received power P_2. Therefore, the measured gain at this frequency is denoted $G(f) = G_{\text{dipole}}(f) + P_2(\text{dBm}) - P_1(\text{dBm})$. Fig. 10 shows the measured and simulated realized gain of the antenna with the proposed active ohmic-FET matching circuit. The antenna operates with a minimum −21.35 dBi at the lower frequency of 200 MHz, while reaching 0.85 dBi at 1.8 GHz. Increased losses of the circuit

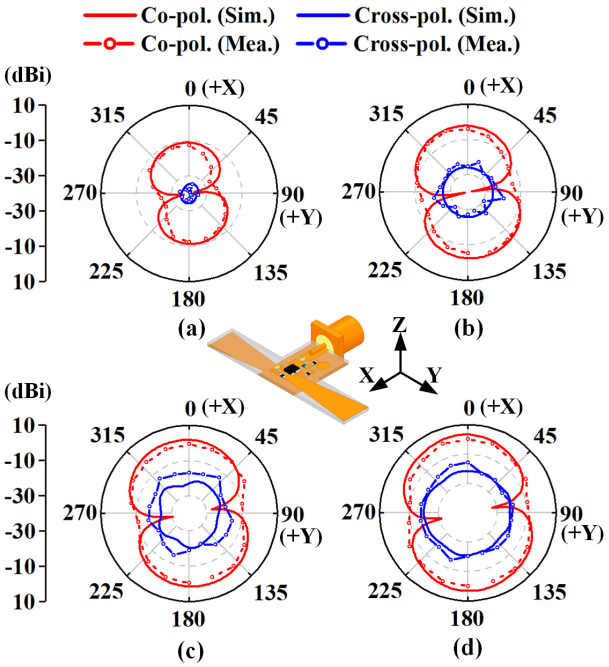

Fig. 11. Measured and simulated radiation patterns at (a) 400 MHz, (b) 800 MHz, (c) 1.2 GHz, and (d) 1.6 GHz.

elements in high frequency cause the measurement results to be lower than the simulated ones. With the ohmic-FET matching circuit, the antenna possesses a significant gain improvement considering its electrically small dimensions. Fig. 11 depicts the radiation patterns at 400 MHz, 800 MHz, 1.2 GHz, and 1.6 GHz. As illustrated in Fig. 11, the radiation patterns perform a typical donut shape of a dipole antenna. This verifies that the proposed ohmic-FET circuit increases the gain by impedance matching without altering its spatial radiation characteristics.

To highlight the performance merits of the proposed active ohmic-FET matching circuit and the matched antenna, Table II summarizes the comparison of the measurement results in this work and other state-of-the-art active antenna designs in open works of literature. The entirety of the listed works aims to achieve a wideband operation with over-octave impedance bandwidth. Sussman-Fort [25], Zhu and Ziolkowski [27], and Sussman-Fort and Rudish [28] adopt the non-Foster circuits for impedance matching, while [30], [32], [34], [35] achieve impedance bandwidth enhancement through amplifiers integration. Antennas reported in [34] and [35] possesses a physical dimension comparable or larger than the wavelength at the operating frequency, which lack the benefits of compact volume. The antennas proposed in [27] and [30] realize wideband with electrically small dimensions. Comparing to our work, the antennas proposed in works [25], [28] and [32] possess a more miniaturized dimension with narrower bandwidths. Besides, their operation bands are at the HF and lower-VHF band, limiting their applications in the mainstream wireless systems at the UHF band. Compared with the previous studies, the active antenna constructed in this work with the ohmic-FET matching circuit performs a significant bandwidth superiority of 190 octaves. Furthermore, the reliability of previous methods is restricted by the operation frequencies of

TABLE II
COMPARISONS OF THE PROPOSED ANTENNA AMONG OTHER ACTIVE ANTENNAS IN THE LITERATURE

Ref.	Method	Volume (λ_0^3)	Center frequency	Bandwidth (%)	Octave bands
[25]	Non-Foster circuit	Length: 0.03	65 MHz	138.46	5.5
[27]	Non-Foster circuit	0.14×11×0.0008	300 MHz	49.2	1.65
[28]	Non-Foster circuit	Length: 0.07	70 MHz	143	6
[30]	LNA integration	0.22×0.22×0.01	5.5 GHz	90.1	2.67
[32]	PA integration	Length: 0.08	12.5 MHz	152	7.33
[34]	LNA integration	1.09×0.6×0.01	3.65 GHz	102.9	3.11
[35]	LNA integration	3.3×2.44×0.02	32.5 GHz	46.2	1.6
This work	**Ohmic-FET matching**	**0.09×0.036×0.0018**	**955 MHz**	**198**	**190**

FETs, of which further bandwidth expansion is challenging. On the other hand, our proposed impedance matching circuit is validated with further bandwidth enhancement potentials by utilizing miniaturized FETs. It is also noticed that because of the electrically small size, the proposed dipole antenna possesses a relatively low radiation gain. This is expected to be improved by changing more types of FETs. In the future, further investigation into the FET's physical parameters can be conducted to expand the matched bandwidth, and break the current limitations of the operation frequency. Moreover, the matching circuit brings potentials to further UWB antenna design. Utilizing this technique, over-hundred-octave antennas with multiple characteristics can be realized in the future, including but not limited to dual-polarized antennas, filtering antennas, and electrically small antennas with directional radiation. In summarize, owing to its operation band, the constructed antenna with ohmic-FET matching circuit covers the widely utilized bands of frequency modulation (FM), digital television (DTV), Global System for Mobile Communications (GSM), and Code Division Multiple Access (CDMA), which ensures application ability in UWB electromagnetic sensing systems.

V. CONCLUSION

In this article, an innovative active circuit is proposed for over-hundred-octave impedance matching of antennas. The core element of this matching circuit is a single FET biased in its ohmic region. To explore the working mechanism of this active matching circuit, an equivalent circuit model is proposed for the ohmic-FET analysis. The model can be divided into the input, transmission, and output parts, with element composition, circuit interaction, and physical nature explained for each part. Based on the model, primary determinants of the bandwidth performances of the circuit are analyzed. As demonstration, a dipole antenna is matched with the proposed ohmic-FET circuit in an ultrawide bandwidth. Parameters study results showcase that the proposed circuit matching bandwidth increases as the integrated ohmic-FET's gate width reduces, while the overall gain elevates as the antenna's dimension enlarges.

A prototype of the dipole antenna integrated with the active ohmic-FET circuit is fabricated and measured, with a compact total dimension of 30 × 12 × 0.6 mm. Experiment results confirm that the proposed active circuit possesses an ultrawide impedance matching bandwidth of 10 MHz–1.9 GHz, covering a 190 octave band. The proposed technique achieves an ultrawide bandwidth of impedance matching and the final product is limited only by the wideband performance of antenna element. This ohmic-FET matching circuit provides a feasible approach for wideband impedance matching in active antennas design, and exhibits promising potentials for UWB electromagnetic sensing tasks in volume-limited systems.

REFERENCES

[1] Y. Zhang and Y. Li, "Wideband microstrip antenna in small volume without using fundamental mode," *Electromagn. Sci.*, vol. 1, no. 2, pp. 1–6, Jun. 2023.

[2] F. Sun, F.-S. Zhang, H. Zhang, H. Zhang, C. Li, and C. Feng, "A frequency diversity printed-Yagi antenna element for apertures selectivity wideband array application," *IEEE Trans. Antennas Propag.*, vol. 66, no. 10, pp. 5634–5638, Oct. 2018.

[3] M. Hu and Y. Li, "Wideband back cover microstrip antenna with multiple shorting vias for mobile 5G MIMO applications," *IEEE Trans. Antennas Propag.*, vol. 71, no. 10, pp. 8290–8295, Oct. 2023.

[4] T. Yin et al., "Wideband high-efficiency transmitarray antenna using compact double-layer dual-linearly polarized elements," *IEEE Antennas Wireless Propag. Lett.*, vol. 22, no. 10, pp. 2372–2376, Oct. 2023.

[5] Y. Zhang, Y. Li, M. Hu, P. Wu, and H. Wang, "Dual-band circular-polarized microstrip antenna for ultrawideband positioning in smartphones with flexible liquid crystal polymer process," *IEEE Trans. Antennas Propag.*, vol. 71, no. 4, pp. 3155–3163, Apr. 2023.

[6] Y. Zhang, Y. Li, W. Zhang, Z. Zhang, and Z. Feng, "Omnidirectional antenna diversity system for high-speed onboard communication," *Engineering*, vol. 11, pp. 72–79, Apr. 2022.

[7] R. C. Qiu and I.-T. Lu, "Multipath resolving with frequency dependence for wide-band wireless channel modeling," *IEEE Trans. Veh. Technol.*, vol. 48, no. 1, pp. 273–285, Jan. 1999.

[8] S. Verdu, "Spectral efficiency in the wideband regime," *IEEE Trans. Inf. Theory*, vol. 48, no. 6, pp. 1319–1343, Jun. 2002.

[9] L. V. Kuz'min, "Noise immunity of the wireless communications scheme based on ultrawideband chaotic radio pulses in multipath channels," *J. Commun. Technol. Electron.*, vol. 56, no. 4, pp. 367–383, Apr. 2011.

[10] W. Sun and Y. Li, "Gain stabilization method for wideband slot-coupled microstrip antenna," *IEEE Trans. Antennas Propag.*, vol. 69, no. 12, pp. 8932–8936, Dec. 2021.

[11] L. J. Chu, "Physical limitations of omni-directional antennas," *J. Appl. Phys.*, vol. 19, no. 12, pp. 1163–1175, Dec. 1948.

[12] W. Geyi, "Physical limitations of antenna," *IEEE Trans. Antennas Propag.*, vol. 51, no. 8, pp. 2116–2123, Aug. 2003.

[13] A. D. Yaghjian and S. R. Best, "Impedance, bandwidth, and Q of antennas," *IEEE Trans. Antennas Propag.*, vol. 53, no. 4, pp. 1298–1324, Apr. 2005.

[14] H. W. Bode, *Network Analysis and Feedback Amplifier Design*. New York, NY, USA: Van Nostrand, 1945.
[15] R. M. Fano, "Theoretical limitations on the broadband matching of arbitrary impedances," *J. Franklin Inst.*, vol. 249, no. 2, pp. 139–154, Feb. 1950.
[16] Z. Zhou et al., "Dispersion coding of ENZ media via multiple photonic dopants," *Light, Sci. Appl.*, vol. 11, no. 1, p. 207, Jul. 2022.
[17] Y. Zhang and Y. Li, "Wideband isotropic antenna with miniaturized ground for enhanced 3 dB coverage ratio," *IEEE Antennas Wireless Propag. Lett.*, vol. 21, no. 6, pp. 1253–1257, Jun. 2022.
[18] W. Sun, Y. Li, Z. Zhang, and P.-Y. Chen, "Low-profile and wideband microstrip antenna using quasi-periodic aperture and slot-to-CPW transition," *IEEE Trans. Antennas Propag.*, vol. 67, no. 1, pp. 632–637, Jan. 2019.
[19] Z. Chen et al., "Compact wideband circularly polarized loop antenna based on dual common and differential modes," *IEEE Antennas Wireless Propag. Lett.*, vol. 21, no. 8, pp. 1567–1571, Aug. 2022.
[20] H. Li, Y. Li, L. Chang, W. Sun, X. Qin, and H. Wang, "A wideband dual-polarized endfire antenna array with overlapped apertures and small clearance for 5G millimeter-wave applications," *IEEE Trans. Antennas Propag.*, vol. 69, no. 2, pp. 815–824, Feb. 2021.
[21] R. K. Singh, A. Basu, and S. K. Koul, "A novel pattern-reconfigurable oscillating active integrated antenna," *IEEE Antennas Wireless Propag. Lett.*, vol. 16, pp. 3220–3223, 2017.
[22] C. H. Mueller et al., "Small-size X-band active integrated antenna with feedback loop," *IEEE Trans. Antennas Propag.*, vol. 56, no. 5, pp. 1236–1241, May 2008.
[23] S.-J. Guo, L.-S. Wu, K. W. Leung, and J.-F. Mao, "Active integrated dielectric resonator antenna-in-package design," *IEEE Antennas Wireless Propag. Lett.*, vol. 18, no. 11, pp. 2414–2418, Nov. 2019.
[24] T.-Y. Shih and N. Behdad, "Wideband, non-foster impedance matching of electrically small transmitting antennas," *IEEE Trans. Antennas Propag.*, vol. 66, no. 11, pp. 5687–5697, Nov. 2018.
[25] S. E. Sussman-Fort, "Matching network design using non-foster impedance," *Int. J. RF Microw. Comput.-Aided Eng.*, vol. 16, pp. 135–143, Feb. 2005.
[26] H.-C. Chen, H.-Y. Yang, C.-C. Kao, and T.-G. Ma, "Slot antenna with non-foster and negative conductance matching in consecutive bands," *IEEE Antennas Wireless Propag. Lett.*, vol. 18, no. 6, pp. 1203–1207, Jun. 2019.
[27] N. Zhu and R. W. Ziolkowski, "Active metamaterial-inspired broadbandwidth, efficient, electrically small antennas," *IEEE Antennas Wireless Propag. Lett.*, vol. 10, pp. 1582–1585, 2011.
[28] S. E. Sussman-Fort and R. M. Rudish, "Non-foster impedance matching of electrically-small antennas," *IEEE Trans. Antennas Propag.*, vol. 57, no. 8, pp. 2230–2241, Aug. 2009.
[29] M.-C. Tang, T. Shi, and R. W. Ziolkowski, "Electrically small, broadside radiating Huygens source antenna augmented with internal non-foster elements to increase its bandwidth," *IEEE Antennas Wireless Propag. Lett.*, vol. 16, pp. 712–715, 2017.
[30] F. Foroutan and N. K. Nikolova, "UWB active antenna for microwave breast imaging sensing arrays," *IEEE Antennas Wireless Propag. Lett.*, vol. 18, no. 10, pp. 1951–1955, Oct. 2019.
[31] K. Cho and S. Hong, "Design of a VHF/UHF/L-band low-power active antenna for mobile handsets," *IEEE Antennas Wireless Propag. Lett.*, vol. 11, pp. 45–48, 2012.
[32] N. Strachen, E. Mohammadi, J. Booske, and N. Behdad, "Active, ultrawideband, electrically small antennas for high-power transmission in the HF band," *IEEE Trans. Antennas Propag.*, vol. 70, no. 3, pp. 1600–1611, Mar. 2022.
[33] F. Giuppi, A. Georgiadis, A. Collado, and M. Bozzi, "A compact, single-layer substrate integrated waveguide (SIW) cavity-backed active antenna oscillator," *IEEE Antennas Wireless Propag. Lett.*, vol. 11, pp. 431–433, 2012.
[34] S. K. Dhar, M. S. Sharawi, O. Hammi, and F. M. Ghannouchi, "An active integrated ultra-wideband MIMO antenna," *IEEE Trans. Antennas Propag.*, vol. 64, no. 4, pp. 1573–1578, Apr. 2016.
[35] H.-R. Zhu, K. Li, J.-G. Lu, and J.-F. Mao, "Millimeter-wave active integrated semielliptic CPW slot antenna with ultrawideband compensation of ball grid array interconnection," *IEEE Trans. Compon., Packag., Manuf. Technol.*, vol. 12, no. 1, pp. 111–120, Jan. 2022.
[36] C. A. Balanis, *Antenna Theory—Analysis and Design*, 4th ed. New York, NY, USA: Wiley, 2016, ch. 4.

Shuyu Wang received the B.S. degree in electronic engineering from Tsinghua University, Beijing, China, in 2022, where he is currently pursuing the Ph.D. degree in electronic engineering.

His current research interests include electrically small antennas, active circuits, and wideband active antennas.

Yue Li (Senior Member, IEEE) received the B.S. degree in telecommunication engineering from Zhejiang University, Hangzhou, Zhejiang, China, in 2007, and the Ph.D. degree in electronic engineering from Tsinghua University, Beijing, China, in 2012.

In June 2012, he was a Post-Doctoral Fellow with the Department of Electronic Engineering, Tsinghua University. In December 2013, he was a Research Scholar with the Department of Electrical and Systems Engineering, University of Pennsylvania, Philadelphia, PA, USA. He was also a Visiting Scholar with the Institute for Infocomm Research (I2R), A*STAR, Singapore, in 2010, and the Hawaii Center of Advanced Communication (HCAC), University of Hawaii at Manoa, Honolulu, HI, USA, in 2012. Since January 2016, he has been with Tsinghua University, where he is currently an Assistant Professor and an Associate Professor with the Department of Electronic Engineering. He has authored and coauthored over 210 journal articles and 50 international conference papers. He holds 26 granted Chinese patents. His current research interests include metamaterials, plasmonics, electromagnetics, nanocircuits, mobile and handset antennas, MIMO and diversity antennas, and millimeter-wave antennas and arrays.

Dr. Li was a recipient of the Issac Koga Gold Medal from URSI General Assembly in 2017, the Second Prize of Science and Technology Award of China Institute of Communications in 2017, the Young Scientist Award from the conferences of Progress in Electromagnetics Research Symposium (PIERS) in 2019, the International Applied Computational Electromagnetics Society Symposium (ACES) in 2018, the Atlantic Radio Science Conference (AT-RASC) in 2018, the Asia–Pacific Radio Science Conference (AP-RASC) in 2016, the International Symposium on Electromagnetic Theory (EMTS) in 2016, and the URSI General Assembly and Scientific Symposium (GASS) in 2014; the Best Paper Award from the conferences of PhotonIcs and Electromagnetics Research Symposium (PIERS) in 2021, the International Workshop on Electromagnetics (iWEM) in 2021, the Asia–Pacific Conference on Antennas and Propagation (APCAP) in 2017 and 2020, the U.K.-Europe-China Workshop on Millimeter Waves and Terahertz Technologies (UCMMT) in 2020, the International Symposium on Antennas and Propagation (ISAP) in 2019, the Cross Strait Quad-Regional Radio Science and Wireless Technology Conference (CSQRWC) in 2018, the International Symposium on Antennas, Propagation and EM Theory (ISAPE) in 2016 and 2021, the International Conference on Microwave and Millimeter Wave Technology (ICMMT) in 2016 and 2020, the National Conference on Microwave and Millimeter Waves (NCMMW) in 2017 and 2018, and the National Conference on Antennas (NCANT) in 2017 and 2019; the Outstanding Doctoral Dissertation of Beijing Municipality in 2013; and the Principal Scholarship of Tsinghua University in 2011. He is serving as an Associate Editor for IEEE TRANSACTIONS ON ANTENNAS AND PROPAGATION, IEEE ANTENNAS AND WIRELESS PROPAGATION LETTERS, *Microwave and Optical Technology Letters*, and *Computer Applications in Engineering Education*. He is also serving on the Editorial Board of *Scientific Reports*, *Sensors*, and *Electronics*.